JOURNAL OF Materials CHEMISTRY

Phase behaviour, magnetic and electronic properties in the series $Co_{1-x}Ni_xCr_2S_4$ $(0 \leqslant x < 1)$†

Paz Vaqueiro, Stefan Sommer and Anthony V. Powell*

Department of Chemistry, Heriot-Watt University, Edinburgh, UK EH14 4AS. E-mail: A.V.Powell@hw.ac.uk

Received 12th May 2000, Accepted 19th July 2000
First published as an Advanced Article on the web 22nd August 2000

Non-stoichiometric phases in the series $Co_{1-x}Ni_xCr_2S_4$ $(0 \leqslant x < 1)$ were prepared at high temperatures. In the composition range $0 \leqslant x \leqslant 0.35$ single-phase materials, isostructural with the end-member spinel $CoCr_2S_4$ are observed, whereas materials in the composition range $0.85 \leqslant x < 1$ adopt the Cr_3S_4 structure of the end-member $NiCr_2S_4$. Rietveld refinements using powder neutron diffraction data demonstrate that in the spinel structure nickel cations are accommodated exclusively at tetrahedral sites and in the Cr_3S_4 phases at octahedral sites in an ordered defect layer. All single-phase materials are semiconductors. Spinel-type phases appear to be ferrimagnetic with saturation moments in the range 2.4–2.6 μ_B, and Curie temperatures which increase with increasing nickel content. The Cr_3S_4-type materials exhibit a magnetic behaviour similar to $NiCr_2S_4$ and Cr_3S_4, which are complex antiferromagnets.

Introduction

Ternary chromium sulfides ACr_2S_4 may, depending on the identity of A, adopt either the spinel[1] (A = Mn, Fe, Co) or the Cr_3S_4 structure[2] (A = Ti, V, Cr, and Ni). In the former, cations occupy both tetrahedral and octahedral interstitial sites in a cubic close packed array of sulfide anions, while in the Cr_3S_4 structure cations occupy octahedral sites between hexagonally close packed sulfide layers. The latter structure can be derived from that of NiAs by removal, in an ordered manner, of cations from octahedral sites between alternate pairs of anion layers, resulting in a change from the ···XMXMXMX··· stacking sequence found in NiAs, to one of ···$XMXM_{1/2}$XMX··· This results in two crystallographically distinct cation sites, as indicated by the formulation (M)[M_2]S_4, where (M) and [M] denote sites in the vacancy and the fully occupied layers respectively. For ACr_2S_4 materials with the spinel or Cr_3S_4 structures, two extreme cation distributions are possible. These correspond to the normal, (A)[Cr_2]S_4, and inverse (Cr)[ACr]S_4 structure types, where parentheses and square brackets respectively represent tetrahedral and octahedral sites in the spinel structure and octahedral sites in the vacancy and fully occupied layers in the Cr_3S_4 structure. The chromium thiospinels ACr_2S_4 have been extensively studied,[1] owing to the combination of semiconducting behaviour and strong ferromagnetism (A = Cd)[3] or ferrimagnetism (A = Mn, Fe, Co)[4,5] which they exhibit, and the influence of magnetic ordering on the resistivity behaviour has been investigated.[6] The recent observation of colossal magnetoresistance (CMR) has led to renewed interest in these materials.[7]

In the spinel structure 1/3 of the cations reside at tetrahedral sites, whilst in the Cr_3S_4 structure all cations are octahedrally coordinated. The latter form therefore has a higher density, and hence thiospinels should undergo a phase transition to a Cr_3S_4 phase at high pressure. It has been shown that heating ACr_2S_4 (A = Mn, Fe, Co) spinels at elevated temperatures and pressures allows isolation of Cr_3S_4 phases by rapid quenching.[8–10] This structural transformation is accompanied by a semiconductor to metal transition[11] as well as by changes in magnetic properties.[12] While the thiospinels show a large increase in the magnetisation below room temperature, the Cr_3S_4 phases exhibit low magnetisation, which is weakly temperature dependent. In the chromium thiospinels with A = Fe, Co, the A^{2+} and Cr^{3+} sublattices are aligned antiparallel since the A–Cr interaction is much stronger than the A–A or Cr–Cr interactions.[5] This gives rise to ferrimagnetic behaviour. Detailed studies on the magnetic structures of ACr_2S_4 (A = Co, Fe, Mn) with the Cr_3S_4 structure have not been carried out, owing to the difficulties in maintaining these phases at ambient pressure. Magnetisation measurements suggest they exhibit a complex magnetic structure similar to that of $NiCr_2S_4$, in which both ferromagnetic and antiferromagnetic Cr–Cr interactions are present.[12]

The pressure and temperature required to effect the spinel to Cr_3S_4 transformation decrease from Mn to Co until,[9] at $NiCr_2S_4$, the Cr_3S_4 phase is stable at ambient temperature and pressure. In an effort to produce materials in which the spinel to NiAs transition may be effected by modest temperatures and pressures, we have studied the solid solution behaviour between $CoCr_2S_4$ and $NiCr_2S_4$, through preparation of materials of the general formula $Co_{1-x}Ni_xCr_2S_4$ $(0 \leqslant x < 1)$. Previous studies of nickel-substituted thiospinels suggest that the spinel phase is stable over a relatively limited range of composition.[13,14] However, the physical properties of these systems have not been studied in detail, and doped phases with the Cr_3S_4 structure have not been reported. In this work, we present a study of the phase behaviour in the series $Co_{1-x}Ni_xCr_2S_4$ over the composition range $0 \leqslant x < 1$, together with structural, magnetic and transport properties of the single-phase materials. *In situ* high pressure and temperature powder neutron diffraction measurements will be carried out shortly to investigate the transformation of the mixed $Co_{1-x}Ni_xCr_2S_4$ spinels to Cr_3S_4-type phases.

Experimental

Materials were synthesised from the elements at elevated temperatures. Mixtures of cobalt (Strem chemicals, 99.8%), nickel (Aldrich, 99.99%), chromium (Aldrich, 99+%), and sulfur (Aldrich, 99.98%) with the appropriate stoichiometry were ground in an agate mortar prior to sealing into evacuated

†Electronic supplementary information (ESI) available: observed, calculated and difference powder neutron diffraction profiles for spinel phases and Cr_3S_4 phases. See http://www.rsc.org/suppdata/jm/b0/b003814h/

Table 1 Results of thermogravimetry and atomic absorption analysis for the single-phase materials

Nominal composition	Nominal Ni content (%)	Experimental Ni content (%)	Nominal Cr content (%)	Experimental Cr content (%)	Expected TGA weight loss (%)	Experimental TGA weight loss (%)	Experimental composition
$Co_{0.9}Ni_{0.1}Cr_2S_4$	2.02	2.04(5)	35.7	35.7(2.0)	22.07	21.69(2)	$Co_{0.91}Ni_{0.10}Cr_{1.99}S_{3.96}$
$Co_{0.8}Ni_{0.2}Cr_2S_4$	4.03	3.97(10)	35.7	35.7(2.0)	22.07	21.59(2)	$Co_{0.82}Ni_{0.20}Cr_{1.98}S_{3.95}$
$Co_{0.7}Ni_{0.3}Cr_2S_4$	6.05	6.12(11)	35.7	34.4(1.9)	22.07	22.46(2)	$Co_{0.76}Ni_{0.30}Cr_{1.94}S_{4.04}$
$Co_{0.65}Ni_{0.35}Cr_2S_4$	7.06	7.16(12)	35.7	35.0(2.0)	22.07	21.38(2)	$Co_{0.70}Ni_{0.35}Cr_{1.95}S_{3.93}$
$Co_{0.15}Ni_{0.85}Cr_2S_{3.93}$	17.3	16.76(28)	36.0	34.4(1.9)	21.47	21.95(2)	$Co_{0.24}Ni_{0.83}Cr_{1.93}S_{3.99}$
$Co_{0.1}Ni_{0.9}Cr_2S_{3.93}$	18.3	17.80(30)	36.0	33.7(1.9)	21.47	22.24(2)	$Co_{0.22}Ni_{0.89}Cr_{1.89}S_{4.0}$
$Co_{0.05}Ni_{0.95}Cr_2S_{3.93}$	19.3	19.64(5)	36.0	35.0(2.0)	21.47	21.80(2)	$Co_{0.08}Ni_{0.97}Cr_{1.95}S_{3.97}$

($<10^{-4}$ Torr) silica tubes. Materials with high nickel contents ($x \geqslant 0.5$) were prepared with a slight deficiency of sulfur, corresponding to a composition of $Co_{1-x}Ni_xCr_2S_{3.93}$, as previous studies have shown that the phase range of the Cr_3S_4 structure does not extend to the fully stoichiometric composition.[15] Mixtures were fired at 800–1000 °C for a period of between 7 and 13 days with intermediate regrinding. Samples were cooled at 4 °C min^{-1} to 300 °C prior to removal from the furnace.

Reaction progress was monitored by powder X-ray diffraction using a Philips PA2000 diffractometer with nickel-filtered Cu-K_α radiation ($\lambda = 1.5418$ Å). The nickel and chromium content of the samples was determined by atomic absorption spectroscopy using an Instrumental Laboratories SII atomic absorption spectrometer. The sulfur content was determined thermogravimetrically by oxidation in a flow of dry oxygen on a Du Pont Instruments 951 thermogravimetric analyzer. The cobalt content was obtained by difference. Time-of-flight powder neutron diffraction data were collected at room temperature on the Polaris diffractometer at ISIS, Rutherford Appleton Laboratory. In each case, data were collected on *ca.* 3 g of sample contained in thin-walled vanadium cans. Initial data manipulation and reduction was carried out using Genie[16] spectrum manipulation software. Neutron diffraction data, from the highest resolution backscattering bank of detectors ($2\theta = 145°$), were summed and normalised for subsequent use in Rietveld refinement using the GSAS package.[17] The electrical resistance of the samples as a function of temperature was measured using the 4-probe DC technique. An ingot ($\approx 6 \times 3 \times 1$ mm) was cut from a sintered pellet, four 50 μm silver wires were attached using colloidal silver paint and connections were made to a HP34401A multimeter. The sample was mounted in an Oxford Instruments CF1200 cryostat connected to an ITC502 temperature controller. Measurements were carried out over the temperature range $77 \leqslant T/K \leqslant 300$. Magnetic measurements were performed using a Quantum Design MPMS2 SQUID susceptometer. Samples were loaded into gelatin capsules at room temperature and data were collected over the temperature range $5 \leqslant T/K \leqslant 300$, both after cooling in zero applied field (zfc) and in the measuring field (fc) of 1000 G. Data were corrected for the diamagnetism of the gelatin capsule. For materials with $x \leqslant 0.35$, magnetisation was measured as a function of the field at 5 K, over the field range $0 \leqslant H/G \leqslant 10000$.

Results

Powder X-ray diffraction demonstrated that in the composition range $0 \leqslant x \leqslant 0.35$ single-phase materials with the spinel structure are observed, whilst in the composition range $0.85 \leqslant x < 1.0$ single phase materials with a Cr_3S_4 structure type are found. At compositions between these two single-phase regions, spinel and Cr_3S_4 type materials coexist. The results of the chemical analysis for the single-phase materials are shown in Table 1. Data are in good agreement with the stoichiometry of the initial reaction mixtures.

Rietveld refinements using powder neutron diffraction data were initiated in the space group $Fd\bar{3}m$ for materials with the spinel structure and in the space group $I2/m$ for materials with the Cr_3S_4 structure. Atomic coordinates previously determined for $CoCr_2S_4$[18] and $NiCr_2S_4$[19] were used for the initial structural models. Cation distributions corresponding to both normal and inverse spinel structures were considered. The background of the neutron profile was modelled with a power series in $Q^{2n}/n!$ and the peak shape was described by a convolution of a pseudo-Voigt with an exponential function. Data in the region 2.10–2.16 Å were excluded from the structural refinements owing to the presence of the (110) reflection of vanadium ($d_{calc} = 2.14$ Å), which is instrumental in origin. Representative final observed, calculated and difference profiles for materials with the spinel and the Cr_3S_4 structures are shown in Fig. 1. Structural refinements for other compositions are of similar quality ($R_{wp} = 1.2$–2%). The refined atomic parameters for materials with the spinel structure are given in Table 2, while those for materials with the Cr_3S_4 structure are given in Table 3. For both single-phase regions lattice parameters and the unit cell volume decrease with increasing Ni content. A decrease in the unit cell volume of *ca.* 8% occurs on going from the spinel single-phase region to the Cr_3S_4 single-phase region. Selected bond lengths and angles are presented in Tables 4 and

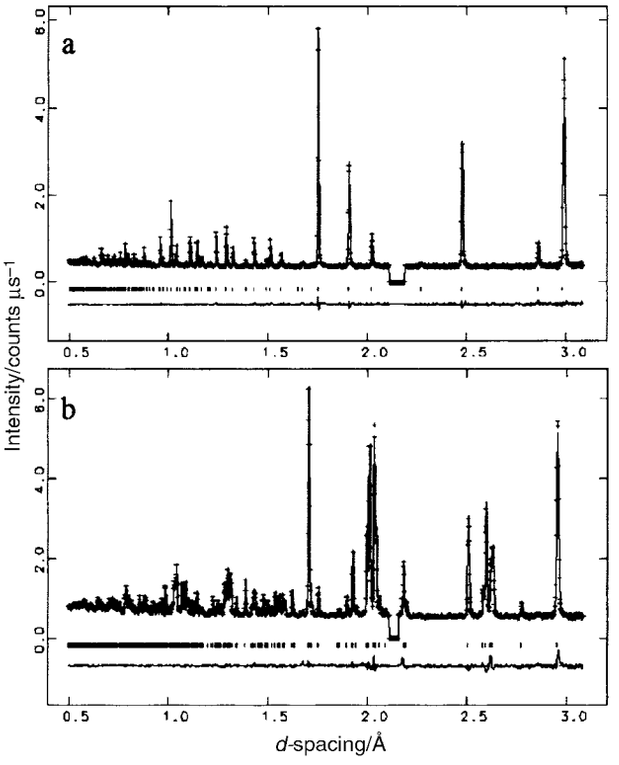

Fig. 1 Observed (crosses), calculated (upper full line) and difference (lower full line) powder neutron diffraction profiles for (a) the spinel-type $Co_{0.7}Ni_{0.3}Cr_2S_4$ and (b) Cr_3S_4 type $Co_{0.1}Ni_{0.9}Cr_2S_4$ phases. Reflection positions are marked.

Table 2 Refined parameters for materials $Co_{1-x}Ni_xCr_2S_4$ with the spinel structure (space group $Fd\bar{3}m$) over the composition range $0 \leqslant x \leqslant 0.35$. Parentheses and square brackets represent tetrahedral and octahedral sites respectively

		x				
		0.0	0.1	0.2	0.3	0.35
	a/Å	9.91792(3)	9.91791(3)	9.91404(2)	9.90414(2)	9.90112(4)
(M)	SOF[b] Co	1.0	0.9	0.8	0.7	0.65
	SOF[b] Ni	0	0.1	0.2	0.3	0.35
	B/Å^2	0.63(1)	0.622(8)	0.669(7)	0.666(7)	0.74(1)
[Cr]	B/Å^2	0.47(2)	0.442(8)	0.458(8)	0.485(8)	0.47(1)
S	x	0.2585(3)	0.2585(2)	0.2584(2)	0.2583(2)	0.2583(3)
	B/Å^2	0.59(2)	0.542(8)	0.550(8)	0.564(8)	0.59(1)
R_{wp} (%)		2.0	1.4	1.3	1.2	1.8
χ^2		1.5	1.3	1.3	1.2	2.1

[a](M) in 8(a): (1/8,1/8,1/8); [Cr] in 16(d): (1/2,1/2,1/2) and S in 32(e): (x,x,x). [b]SOF: Site occupancy factor.

5. Polyhedral volumes were calculated with the program Volcal.[20]

The resistivity (ρ) of non-stoichiometric materials with the spinel structure exhibits a strong temperature dependence (Fig. 2). The negative slope $d\rho/dT$ indicates semiconducting behaviour, although the temperature dependence of the resistivity does not follow an Arrhenius law. With increasing nickel content, the resistivity at a given temperature decreases, and in the composition range $0.2 < x \leqslant 0.35$ the resistivity at 80 K is only 2% of the value for $CoCr_2S_4$ at the same temperature. In the composition range $0 \leqslant x \leqslant 0.2$ a change in slope of $\ln \rho$ *vs.* $1/T$ occurs over a temperature range in the region of the magnetic ordering temperature (Fig. 3a). Similar behaviour has previously been reported for p-type polycrystalline $CoCr_2S_4$.[21] In the composition range $0.2 < x \leqslant 0.35$ plots of $\ln \rho$ *vs.* $T^{-1/4}$ are linear over a wide temperature range, consistent with a variable range hopping conduction mechanism (Fig. 3b). Non-stoichiometric single-phase materials with the Cr_3S_4 structure are semiconductors with a weak temperature dependence (Fig. 4). Plots of $\ln \rho$ *vs.* $1/T$ are linear over the temperature range $77 \leqslant T/K \leqslant 200$, indicating Arrhenius-like behaviour. The activation energies derived from these plots are given in Table 6. These values are comparable to those reported for $NiCr_2S_4$ below the magnetic ordering temperature.[22]

Materials with the two structure types exhibit contrasting magnetic behaviour (Fig. 5). The thiospinels ($0 \leqslant x \leqslant 0.35$) show a large increase in the magnetisation at temperatures below 250 K. The appearance of the $\sigma(T)$ curves is similar to that reported previously for $CoCr_2S_4$, which is a ferrimagnet with $T_C \approx 240$ K.[5] The magnetic ordering temperatures, determined by extrapolation of the steepest slope of the magnetisation curve to zero magnetisation, increase slightly with increasing nickel content. The magnetisation as a function of the applied field at 5 K for the doped thiospinels is presented in Fig. 6. The saturation magnetisation was determined by extrapolation to infinite field in the plots of magnetisation *vs.* $1/H$. The derived magnetic parameters are given in Table 7. The magnetisation of materials with the Cr_3S_4 structure exhibits a weak temperature dependence. In the composition range $0.85 < x < 1$, fc and zfc curves overlie each other completely, and the magnetisation over the temperature range $200 \leqslant T/K \leqslant 300$ is almost independent of temperature. With decreasing temperature, the magnetisation reaches a minimum value at *ca.* 110 K, and then increases as the temperature decreases further. Data in the high temperature region could not be fitted using a Curie–Weiss law. The form of these curves is similar to that previously reported for $NiCr_2S_4$,[23] which orders magnetically at 180 K.[24,25] Although X-ray and neutron diffraction data suggest that the material $Co_{0.15}Ni_{0.85}Cr_2S_4$ is a single phase with the Cr_3S_4 structure, magnetisation data are consistent with the presence of trace amounts (*ca.* 0.1%) of a thiospinel phase, which is below the limits of detection by powder diffraction methods.

Table 3 Refined parameters for materials $Co_{1-x}Ni_xCr_2S_4$ with the Cr_3S_4 structure (space group $I2/m$) over the composition range $0.85 \leqslant x < 1$. Parentheses and square brackets represent octahedral sites in the vacancy and fully occupied layers respectively

		x		
		0.85	0.90	0.95
a/Å		5.90290(6)	5.90015(5)	5.89997(5)
b/Å		3.41133(3)	3.41171(3)	3.41189(3)
c/Å		11.0901(1)	11.08912(9)	11.08990(9)
β/°		91.272(1)	91.303(1)	91.332(1)
(M)	SOF[b] Ni	0.85	0.90	0.95
	SOF[b] Co	0.15	0.10	0.05
	B/Å^2	0.679(9)	0.711(9)	0.707(9)
[Cr]	x	−0.0205(1)	−0.0204(1)	−0.0200(1)
	z	0.26128(7)	0.26148(6)	0.26173(7)
	B/Å^2	0.40(1)	0.37(1)	0.34(1)
S(1)	x	0.3420(2)	0.3424(2)	0.3426(2)
	z	0.36526(9)	0.36541(9)	0.36524(9)
	B/Å^2	0.33(1)	0.33(1)	0.32(1)
S(2)	x	0.3296(2)	0.3300(2)	0.3297(2)
	z	0.88092(8)	0.88089(8)	0.88100(8)
	B/Å^2	0.35(1)	0.38(1)	0.35(1)
R_{wp} (%)		1.2	1.3	1.5
χ^2		2.1	2.3	2.9

[a](M) in 2(a): (0,0,0); [Cr], S(1) and S(2) in 4(i): (x,0,z). [b]SOF: Site occupancy factor.

Discussion

The solid-solution behaviour observed in the nickel-doped thiospinels is in agreement with previous reports,[13] and comparable to that of $A_{1-x}Ni_xCr_2S_4$ with A = Mn, Fe, Zn.[13,14] The relatively narrow range of solubility of Ni^{2+} in the thiospinels has been attributed to the strong preference of this cation for the octahedral sites,[26] which combined with the strong octahedral preference of Cr^{3+}, would stabilise the Cr_3S_4 structure containing only octahedral cation sites. The solid solution range for the Cr_3S_4 type materials in $Co_{1-x}Ni_xCr_2S_4$ is even narrower, but comparable to that observed in $Cr_{3-x}A_xS_4$ (A = Mn, Fe, Co) when the materials were cooled slowly.[27] However, in the latter system quenching of the samples from 1000 °C gives rise to a remarkable increase in the amount of A cations incorporated into the Cr_3S_4 phase. In particular, for $Cr_{3-x}Co_xS_4$ less than 10 mol% of Co can be incorporated when the samples are slowly cooled, while a solubility of *ca.* 50% is achieved by quenching from 1000 °C. A similar behaviour in the system $Co_{1-x}Ni_xCr_2S_4$ cannot be excluded.

Previous neutron diffraction studies of stoichiometric ACr_2S_4 thiospinels (A = Mn, Fe, Co)[18] have shown that they exhibit the normal structure type, as a consequence of the strong octahedral preference of Cr^{3+}. The cation distribution of nickel-doped thiospinels has never been investigated, and

Table 4 Selected distances (Å) and angles (°) for $Co_{1-x}Ni_xCr_2S_4$ compositions with the spinel structure. Parentheses and square brackets represent tetrahedral and octahedral sites respectively

	x				
	0.0	0.1	0.2	0.3	0.35
(M)–S	2.2932(5) × 4	2.2929(4) × 4	2.2908(4) × 4	2.2859(4) × 4	2.2863(6) × 4
[Cr]–S	2.3982(3) × 6	2.3983(2) × 6	2.3981(2) × 6	2.3971(2) × 6	2.3957(3) × 6
[Cr]–[Cr]	3.50651(1) × 6	3.50651(1) × 6	3.50514(1) × 6	3.50164(1) × 6	3.50057(1) × 6
S–(M)–S	109.471(-) × 6	109.471(-) × 6	109.471(-) × 6	109.471(-) × 6	109.471(-) × 6
S–[Cr]–S	85.91(2) × 6	85.91(1) × 6	85.95(1) × 6	86.03(1) × 6	85.99(2) × 6
	94.09(2) × 6	94.09(1) × 6	94.05(1) × 6	93.97(1) × 6	94.01(2) × 6

given the preference of Ni^{2+} for octahedral sites, these materials could exhibit a partially inverted structure. However, for the nickel-doped thiospinels prepared in this work, structural models with Ni in the octahedral sites and Cr in the tetrahedral sites resulted in Rietveld refinements with significantly higher R_{wp} factors than the structural model based on a normal structure. Subsequent refinement of Ni and Cr site occupancy factors at both sites, with the constraint that overall stoichiometry was maintained, resulted in site occupancy factors close to zero for Cr on the tetrahedral sites and for Ni on the octahedral site. Therefore, it can be concluded that these materials also exhibit the normal structure type. Ordering of the A cations on the tetrahedral sites, which lowers the space group from $Fd\bar{3}m$ to $F\bar{4}3m$, has been reported for some chromium thiospinels such as $Cu_{0.5}Fe_{0.5}Cr_2S_4$ and $Cu_{0.5}In_{0.5}Cr_2S_4$.[1,28] However, no ordering of the Ni and Co cations was observed in the system $Co_{1-x}Ni_xCr_2S_4$. For the single-phase materials with the Cr_3S_4 structure, structural refinements in which Ni and Cr were allowed to occupy both layers, with the constraint that overall stoichiometry was maintained, resulted in *ca.* 3% of Cr cations in the vacancy layer. In spite of this, no significant improvement in the goodness of fit indicator was observed. Therefore, Cr_3S_4-type materials exhibit a structure of the normal type. The cation distribution of these samples differs slightly from that of $NiCr_2S_4$ determined previously, in which *ca.* 15% of Cr cations reside in the vacancy layer.[19] A high temperature neutron diffraction study of this material demonstrated that the cation distribution is dependent on the preparation conditions, in particular the cooling rate.[29]

Table 5 Selected distances (Å) and angles (°) for $Co_{1-x}Ni_xCr_2S_4$ compositions with the Cr_3S_4 structure. Parentheses and square brackets represent octahedral sites in the vacancy and fully occupied layers respectively

	x		
Bonds	0.85	0.90	0.95
(M)–S(1)	2.4393(7) × 4	2.4370(7) × 4	2.4376(7) × 4
(M)–S(2)	2.376(1) × 2	2.377(1) × 2	2.376(1) × 2
Mean (M)–S	2.42	2.42	2.42
[Cr]–S(1)	2.408(1)	2.408(1)	2.404(1)
	2.4606(9) × 2	2.4616(8) × 2	2.4612(9) × 2
[Cr]–S(2)	2.385(1)	2.387(1)	2.389(1)
	2.3463(9) × 2	2.3444(9) × 2	2.3452(9) × 2
Mean [Cr]–S	2.40	2.40	2.40
(M)–[Cr]	2.9029(7) × 2	2.9048(7) × 2	2.9077(7) × 2
[Cr]–[Cr]	3.207(1) × 2	3.207(1) × 2	3.211(1) × 2
	3.41133(3) × 2	3.41171(3) × 2	3.41189(3) × 2
	3.634(1) × 2	3.632(1) × 2	3.629(1) × 2
S(1)–(M)–S(1)	88.73(3) × 2	88.85(3) × 2	88.83(3) × 2
	91.27(3) × 2	91.148(3) × 2	91.17(3) × 2
S(1)–(M)–S(2)	88.06(3) × 4	88.03(2) × 4	87.97(3) × 4
	91.94(3) × 4	91.97(3) × 4	92.03(3) × 4
S(1)–[Cr]–S(1)	83.45(4) × 2	83.54(4) × 2	83.54(4) × 2
	87.77(4)	87.74(4)	87.76(4)
S(1)–[Cr]–S(2)	94.10(4) × 2	94.12(3) × 2	94.28(4) × 2
	87.36(4) × 2	87.24(3) × 2	87.13(3) × 2
	89.44(2) × 2	89.41(2) × 2	89.42(3) × 2
S(2)–[Cr]–S(2)	94.66(3) × 2	94.66(3) × 2	94.61(3) × 2
	93.27(5)	93.38(5)	93.34(5)

In the spinel phase region, with increasing Ni content the cubic unit cell parameter is reduced relative to that of $CoCr_2S_4$. This is in agreement with expectations based on the magnitude of the respective ionic radii ($r_{Co} = 0.58$ Å, $r_{Ni} = 0.55$ Å).[30] The metal–sulfur distances also decrease with increasing Ni content. This reduction is more pronounced for the tetrahedral A–S distances than for the octahedral Cr–S distances, as expected for nickel substitution on the tetrahedral site. As a consequence, the volume of the Cr-centred octahedra decreases by only *ca.* 0.2% in the single-phase region while the volume of the tetrahedra falls by *ca.* 1%. This behaviour is in accord with studies on ternary chromium thiospinels ACr_2S_4 (A = transition metal), which have found that the Cr–S distances are practically independent of A, with the exception of the Cu compound.[1] This is reflected in the different transport properties exhibited by the latter material.[31] The lattice parameters determined for the Cr_3S_4-type phases are similar to those of isostructural materials, such as Cr_3S_4[15] or $NiCr_2S_4$.[19] With increasing Co content the unit cell volume increases, owing to the larger ionic radii of the Co^{2+} cation. Calculations of the volume of the octahedra show that whilst the volume of the Cr-centred octahedra (in the fully occupied layer) remains constant, that of the A-site (in the vacancy layer) increases to accommodate the larger Co cations.

One-electron one-molecule energy level diagrams for AB_2S_4 materials with the spinel[32] and Cr_3S_4[33] structures show that metallic behaviour can result from direct overlap of the t_{2g} orbitals, or from the formation of partially filled narrow energy bands of antibonding σ_A^* or σ_B^* states, produced by covalent mixing of cation d states and anion s and p states. In ACr_2S_4 materials, the Cr–Cr distances are always larger than R_c, the critical distance for t_{2g} direct orbital overlap, leading to localisation of the t_{2g} states. However the vacant e_g states of the Cr^{3+} ions are broadened into σ_B^*-band states. Goodenough

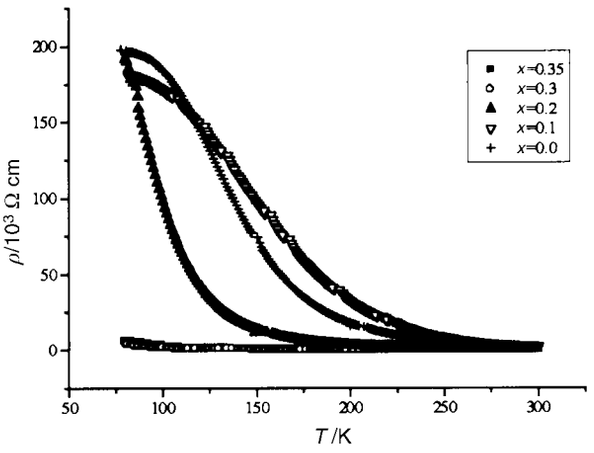

Fig. 2 Temperature dependence of the electrical resistivity for $Co_{1-x}Ni_xCr_2S_4$ materials with the spinel structure.

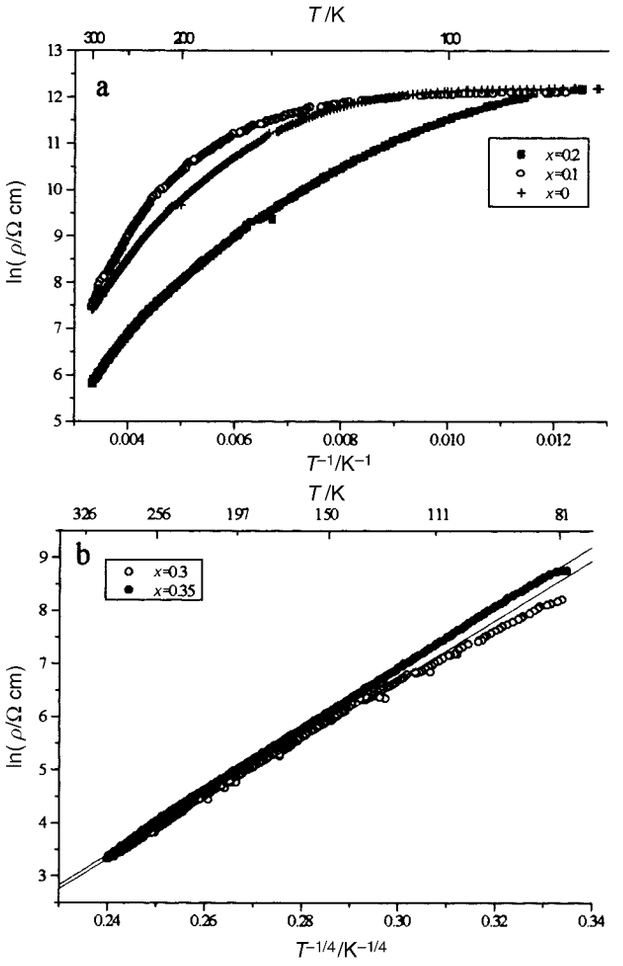

Fig. 3 (a) Arrhenius plot for thiospinels over the composition range $0 \leqslant x \leqslant 0.2$ and (b) $T^{-1/4}$ dependence of $\ln \rho$ for materials over the composition range $0.2 < x \leqslant 0.35$. The straight lines are the fit to a variable range hopping expression.

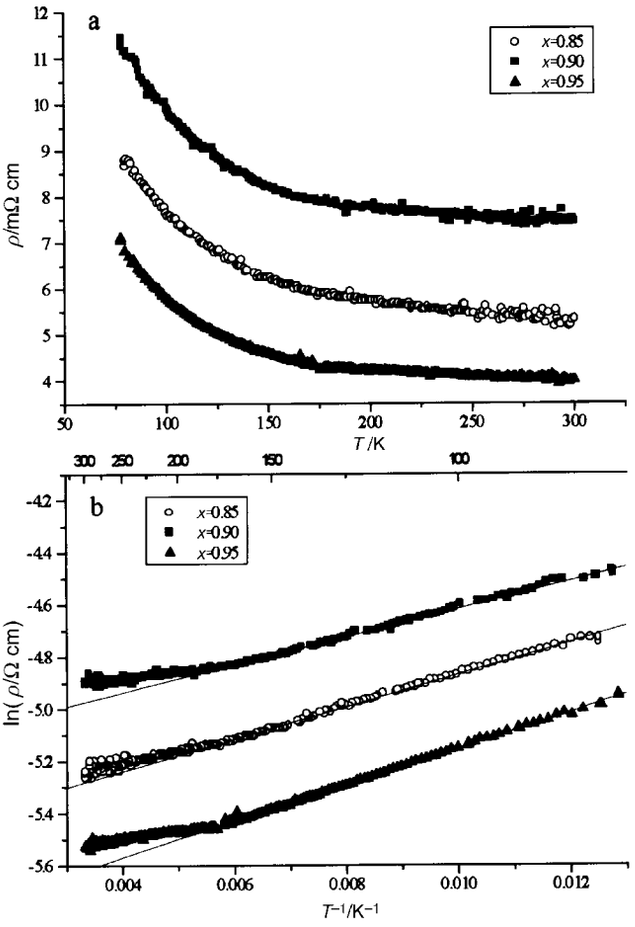

Fig. 4 Temperature dependence of the electrical resistivity for $Co_{1-x}Ni_xCr_2S_4$ materials with the Cr_3S_4 structure: (a) resistivity as a function of temperature; (b) Arrhenius plot showing the linear fits to data below the magnetic ordering temperature.

has shown that in $CoCr_2S_4$ the tetrahedral site Co^{2+} can be described by a ligand-field model,[32] in which both t_{2g} and e_g states are localised, leading to semiconducting behaviour. Substitution of Co by Ni will introduce electrons in localised states and consequently the non-stoichiometric materials will remain semiconducting. For the other end-member ($NiCr_2S_4$), the octahedral site Ni^{2+} can also be described by a ligand-field model, but the covalent mixing parameter λ_σ is close to the critical value, λ_c, required for the formation of σ_A^*-band states. As a consequence, the activation energy for electron transport is small and $NiCr_2S_4$ is a low-activation-energy semiconductor. As both the e_g and t_{2g} levels are localised, substitution of Ni by Co will introduce holes in localised energy levels, and therefore no changes in the transport properties should be expected.

Although the rigid band model can explain why the nickel-doped thiospinels remain semiconducting, it cannot explain the marked reduction in resistivity observed in the composition range $0.2 < x \leqslant 0.35$ nor the change in the temperature dependence, which follows a variable-range-hopping conduction mechanism in this composition range. The decrease in resistivity suggests that with increasing Ni content the materials are approaching an insulator–metal boundary, while the variable-range hopping behaviour indicates that the substitutional disorder on the tetrahedral sites plays an important role in the transport mechanism.

The magnetic behaviour of $CoCr_2S_4$ has been interpreted in terms of ferrimagnetism in which the Co^{2+} spins on the tetrahedral sites are coupled antiparallel to the Cr^{3+} spins on the octahedral sites in a collinear Néel configuration.[5] The saturated moment per molecule extrapolated to 0 K has been estimated by several authors to be in the range 2.4–2.5 μ_B.[1] Gibart *et al.*[5] have determined that the *g*-factor for the tetrahedral Co^{2+} ions is 2.3–2.38, and as a result the Co^{2+} ions have a moment of 3.45–3.57 μ_B, which opposes a moment of 6 μ_B on the Cr^{3+} ions. This gives a resultant moment of 2.55–2.43 μ_B, in good agreement with the values determined experimentally. Substitution by Ni at the tetrahedral sites will decrease the moment on the tetrahedral site by *ca.* 0.1 μ_B for every 0.1 step in *x*, leading to a comparable increase in the resultant saturated moment. The saturation magnetisation values determined for the $Co_{1-x}Ni_xCr_2S_4$ spinel phases (Table 7) appear to be approximately in accord with this, although a slight decrease in the moment is observed for $x = 0.20$.

In the magnetisation curves of the doped thiospinels (Fig. 6), a change in the behaviour at low fields can be observed for the material with the highest doping level ($x = 0.35$). This suggests that in this case the magnetic ground state differs from that of $CoCr_2S_4$. In the spinels ACr_2X_4 (X = O, S, Se) there are three types of Cr–Cr magnetic interactions: an antiferromagnetic

Table 6 Activation energies derived from the Arrhenius plots for materials with the Cr_3S_4 structure. The activation energy for $NiCr_2S_4$ below the magnetic ordering temperature was taken from ref. 25

Composition	$E_a/10^{-3}$ eV
$NiCr_2S_4$	2.12(2)
$Co_{0.05}Ni_{0.95}Cr_2S_4$	5.39(3)
$Co_{0.10}Ni_{0.90}Cr_2S_4$	4.69(3)
$Co_{0.15}Ni_{0.85}Cr_2S_4$	6.02(2)

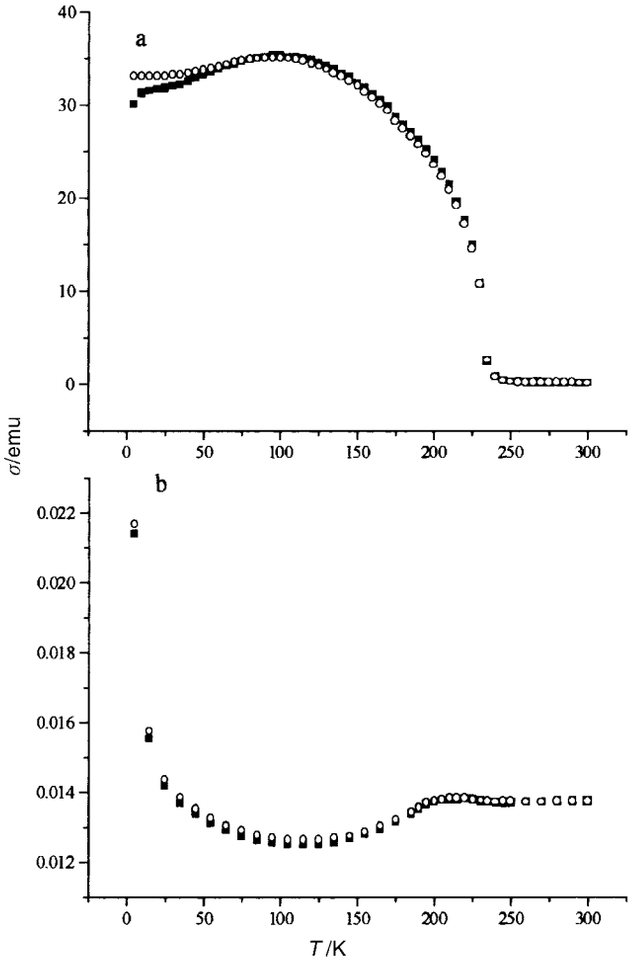

Fig. 5 Temperature dependence of the zero-field cooled (solid squares) and field-cooled (open circles) magnetisation per gram (σ) for representative single-phase $Co_{1-x}Ni_xCr_2S_4$ materials: (a) with the spinel structure ($Co_{0.7}Ni_{0.3}Cr_2S_4$); and (b) the Cr_3S_4 structure ($Co_{0.1}Ni_{0.9}Cr_2S_4$).

exchange interaction caused by the direct overlap of the Cr^{3+} ions, a ferromagnetic Cr–X–Cr superexchange interaction and an antiferromagnetic Cr–X–X–Cr interaction. In the oxyspinels the antiferromagnetic Cr–Cr interaction predominates, but in sulfides the Cr–Cr distances are larger and therefore the superexchange interactions become predominant. A molecular field analysis of the magnetic data of $CoCr_2S_4$[5] concluded that the dominant exchange interaction in this material is that between Cr^{3+} and Co^{2+}, which is negative, while the Cr–Cr

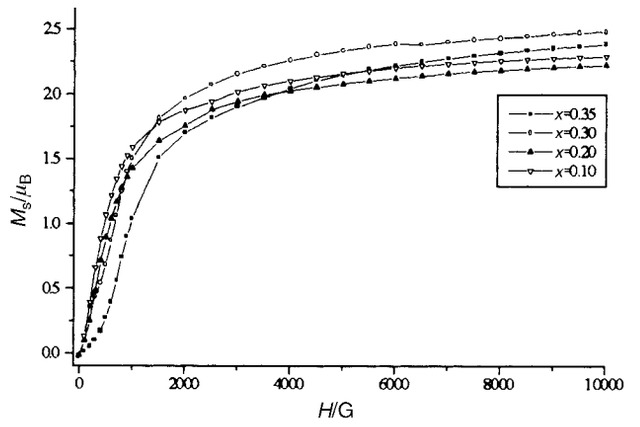

Fig. 6 Magnetisation as a function of field for $Co_{1-x}Ni_xCr_2S_4$ materials with the spinel structure ($0.1 \leqslant x \leqslant 0.35$) at 5 K.

Table 7 Curie temperature and saturation magnetisation at 5 K for the thiospinels $Co_{1-x}Ni_xCr_2S_4$ with $0 \leqslant x \leqslant 0.35$

Composition	T_C/K	Saturation magnetisation/μ_B
$CoCr_2S_4$	230(10)	—
$Co_{0.9}Ni_{0.1}Cr_2S_4$	230(5)	2.412(5)
$Co_{0.8}Ni_{0.2}Cr_2S_4$	233(5)	2.361(5)
$Co_{0.7}Ni_{0.3}Cr_2S_4$	236(5)	2.603(6)
$Co_{0.65}Ni_{0.35}Cr_2S_4$	240(5)	2.613(6)

interaction is very weak. This is caused by the competition between positive Cr–X–Cr and negative Cr–X–X–Cr interactions. A slight change in the relative magnitude of these interactions could give rise to a spiral ground state, such as those observed in $ZnCr_2Se_4$[34] or in the metamagnet $HgCr_2S_4$.[35] The magnetisation as a function of temperature for materials with the Cr_3S_4 structure is very similar to that of $NiCr_2S_4$, and suggests that these materials have the same magnetic structure. This can be described in terms of ferromagnetic sheets parallel to the $(10\bar{1})$ planes, which in turn are coupled antiferromagnetically which respect to each other.[24,25]

Acknowledgements

We wish to thank the EPRSC for a research grant in support of our neutron scattering programme. One of the authors (P.V.) thanks The Leverhulme Trust for a research fellowship. The assistance of Dr R.I. Smith, Rutherford Appleton Laboratory, with the collection of powder neutron diffraction data is gratefully acknowledged.

References

1 R. P. van Stapele, in *Ferromagnetic Materials*, vol. 3, ed. E. P. Wohlfarth, North-Holland Publishing Company, Amsterdam, 1982, ch. 8.
2 C. N. R. Rao and K. P. R. Pisharody, *Prog. Solid State Chem.*, 1979, **10**, 207.
3 N. Menyuk, K. Dwight, R. J. Arnott and A. Wold, *J. Appl. Phys.*, 1966, **37**, 1387.
4 N. Menyuk, K. Dwight and A. Wold, *J. Appl. Phys.*, 1965, **36**, 1088.
5 P. Gibart, J. L. Dormann and Y. Pellerin, *Phys. Status Solidi*, 1969, **36**, 187.
6 P. F. Bongers, C. Haas, A. M. J. G. van Run and G. Zanmarchi, *J. Appl. Phys.*, 1969, **40**, 958.
7 A. P. Ramirez, R. J. Cava and J. Krajewski, *Nature*, 1997, **386**, 156.
8 W. Albers and C. J. M. Roymans, *Solid State Commun.*, 1965, **3**, 417.
9 R. E. Tressler, F. A. Hummel and V. S. Stubican, *J. Am. Ceram. Soc.*, 1968, **51**, 648.
10 R. J. Bouchard, *Mater. Res. Bull.*, 1967, **2**, 459.
11 W. Albers, G. van Aller and C. Haas, in *Propriétés Thermodynamiques Physiques et Structurales des Dérivés Semi-Metalliques*, CNRS, Paris, 1967.
12 R. E. Tressler and V. S. Stubican, *J. Am. Ceram. Soc.*, 1968, **51**, 391.
13 M. Robbins, P. Gibart, D. W. Johnson, R. C. Sherwood and V. G. Lambrecht, *J. Solid State Chem.*, 1974, **9**, 170.
14 H. Itoh, K. Motida and S. Miyahara, *J. Phys. Soc. Jpn.*, 1977, **43**, 854.
15 F. Jellinek, *Acta Crystallogr.*, 1957, **10**, 620.
16 W. I. F. David, M. W. Johnson, K. J. Knowles, C. M. Moreton-Smith, G. D. Crisbie, E. P. Campbell, S. P. Graham and J. S. Lyall, Rutherford Appleton Laboratory Report, RAL-86-102, 1986.
17 A. C. Larson and R. B. von Dreele, General Structure Analysis System, Los Alamos Laboratory, [Report LAUR 85-748], 1994.
18 P. M. Raccah, R. J. Bouchard and A. Wold, *J. Appl. Phys.*, 1966, **37**, 1436.
19 D. C. Colgan and A. V. Powell, *J. Mater. Chem.*, 1997, **7**, 2433.
20 L. W. Finger and Y. Ohashi, CCP14 crystallographic software, http://www.ccp14.ac.uk/.
21 R. J. Bouchard, P. A. Russo and A. Wold, *Inorg. Chem.*, 1965, **4**, 685.

22 R. J. Bouchard and A. Wold, *J. Phys. Chem. Solids*, 1966, **27**, 591.
23 B. L. Morris, P. Russo and A. Wold, *Phys. Chem. Solids*, 1970, **31**, 635.
24 B. Andron and E. F. Bertaut, *J. Phys. (Paris)*, 1966, **27**, 619.
25 A. V. Powell, D. C. Colgan and C. Ritter, *J. Solid State Chem.*, 1997, **134**, 110.
26 A. Miller, *J. Appl. Phys.*, 1959, **30**, 24S.
27 H. D. Lutz, U. Koch and H. Siwert, *Mater. Res. Bull.*, 1983, **18**, 1383.
28 F. K. Lotgering, R. P. Van Stapele, G. H. A. M. Van der Steen and J. S. Van Wieringen, *J. Phys. Chem. Solids*, 1969, **30**, 799.
29 P. Vaqueiro, S. Hull, B. Lebech and A. V. Powell, *J. Mater. Chem.*, 1999, **9**, 2859.
30 R. D. Shannon, *Acta Crystallogr., Sect. A*, 1976, **32**, 751.
31 F. K. Lotgering, *Solid State Commun.*, 1964, **2**, 55.
32 J. B. Goodenough, in *Propriétés Thermodynamiques, Physiques et Structurales des Dérives Semi-Metalliques*, CNRS, Paris, 1967.
33 S. L. Holt, R. J. Bouchard and A. Wold, *J. Phys. Chem. Solids*, 1966, **27**, 755.
34 R. Plumier, *J. Appl. Phys.*, 1966, **37**, 964.
35 P. K. Baltzer, P. J. Wojtowiicz, M. Robbins and E. Lopatin, *Phys. Rev.*, 1966, **151**, 367.